Noname manuscript No.
(will be inserted by the editor)

Modelling of cable-driven continuum robots with general cable routing: A comparison

Soumya Kanti Mahapatra · Ashwin K. P. · Ashitava Ghosal

Received: date / Accepted: date

Abstract Accurate modelling of continuum robots is required for predicting its motion and for model based control. In this work, we restrict our study to cable actuated continuum robots with a flexible backbone on which perforated disks are fixed and through which a cable is routed from the base to the tip. We compare two well known models, namely the optimization-based model and the more extensively used Cosserat rod model for kinematic analysis. Both the models can predict the shape and motion of a cable-driven continuum robot (CCR) with cable routed in a general manner. The paper focuses on comparing these two models based on their ease of modelling and simulation. It was found that the optimization-based method is comparatively faster than the Cosserat rod model for most of the real world cases. These two methods are also compared with experimental results obtained with a 3D printed prototype continuum robot. It is observed that both the methods can reasonably accurately predict the shape with the optimization-based method performing better by a small amount.

Keywords Continuum robot · cable-driven · tendon-driven · kinematics model · generally routed cable

1 Introduction

With the need for better reachability, manoeuvrability and inherent compliance, continuum robots are becoming more common for applications involving congested spaces and handling of delicate objects. Continuum robots are

S. K. Mahapatra and A. Ghosal*
Department of Mechanical Engineering, Indian Institute of Science, Bangalore, Karnataka 560012, India. E-mail: soumyam@iisc.ac.in, asitava@iisc.ac.in. *Corresponding author

Ashwin K. P.
Department of Mechanical Engineering, BITS Pilani K.K. Birla Goa Campus, Goa 403726, India. E-mail: ashwinp@goa.bits-pilani.ac.in

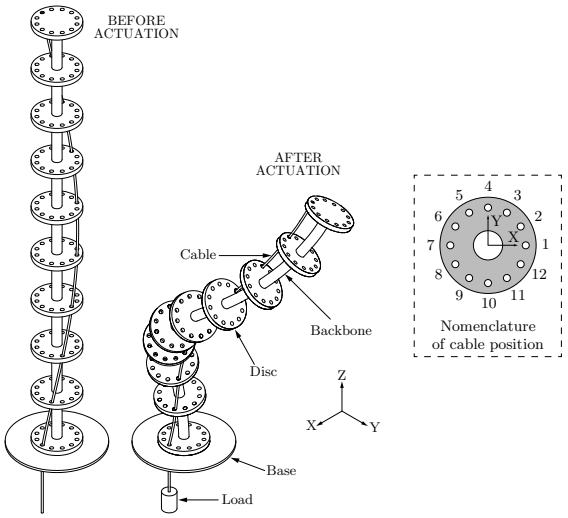

Fig. 1 Schematics of a CCR before and after actuation.

characterized by an elastic backbone which is actuated in various ways – pneumatic, shape-memory alloys, pre-curved beams and cables are some the well-known ways. Cable-driven continuum robots (CCR) or tendon-driven continuum robots are widely studied for their simplicity in design and scalability and find use in fields such as medical devices, remote inspections, search and rescue, space applications, biomimetics etc. [1]. The CCR usually consists of a slender rod like structure forming the *backbone* and circular disks, with holes arranged in a circle, are attached at equal intervals along the backbone (see Fig. 1). Cables are routed through these holes and attached to the top-most disk, and when these cables are actuated from the bottom, the whole CCR bends and takes various shapes depending on the routing of the cable.

Accurate modelling of CCR is essential in correctly predicting the shape and behaviour of a CCR. Detailed review of such models can be found in [2,3]. The simplest models employ geometry based methods that use the constant curvature approach [4]. More sophisticated models use finite element models [5, 6], elasticity based methods considering cable friction [7], Euler-Bernoulli beam theory [8], Cosserat rod theory [9,10], pseudo-rigid body model [11], Euler-Lagrange formulation [12], principle of virtual power [13] and geometry-based optimization method [14] to name a few. Most of the models of CCRs focus on cables which are routed straight. Even though this makes the models simpler, with straight routing, a CCR cannot attain complicated shapes that a generally routed CCR can achieve. The optimization-based method and Cosserat rod model are capable of accurately predicting the shape of CCRs with generally routed cable. This paper focuses on these two approaches and presents the advantages and disadvantages in modelling and simulation of the kinematics of a generally routed CCR. We also compare the simulations results from these

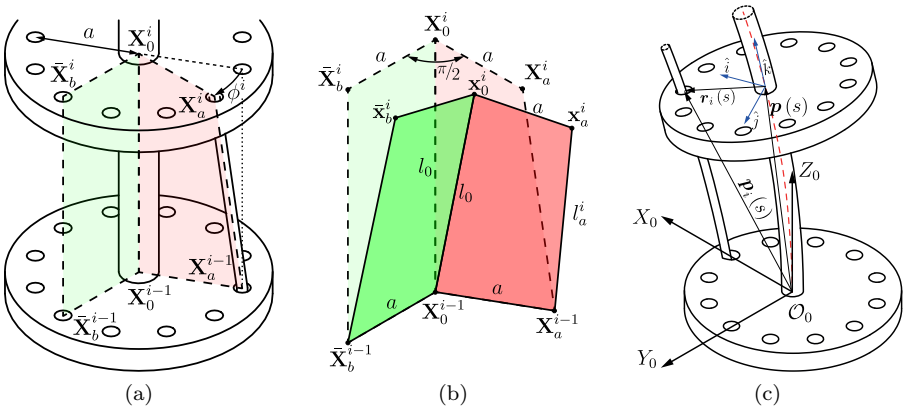

Fig. 2 (a) Nomenclature for optimization-based method, (b) Four bars before (in lighter shade) and after actuation (in darker shade), (c) Nomenclature for Cosserat rod model

two models with experimental results obtained from a 3D printed prototype, again to judge their accuracy in predicting the shape of an actuated CCR.

The rest of the paper is organized as follows: In section 2, a brief summary of the optimization-based and Cosserat rod modelling is presented. In section 3, a comparison between the two methods are presented and then the results are compared with a 3D printed CCR prototype. Lastly in section 4, concluding remarks along with scope for future work are presented.

2 Generally routed CCR with a single cable

In this section, we present a brief overview of the optimization-based method and Cosserat rod model for the kinematics of a CCR with single generally routed cable. More details on the optimization and Cosserat rod modelling approaches can be found in references [14,9].

Optimization-based model: In the optimization-based method, the CCR is discretized as four bar linkages, stacked one on top of the other with each four bar lying in between two consecutive disks. At any particular disk, the position of the center of a disk and location of the cable is denoted by $\mathbf{X}_0^{(\cdot)}$ and $\mathbf{X}_a^{(\cdot)}$, respectively with the superscript denoting the disk number starting with $i = 0$ for the base disk. Inside each segment an imaginary four-bar linkage is assumed consisting of the two disks, the backbone and the cable. Figure 2a shows the i^{th} section with the four bar $\mathbf{X}_0^{i-1}\mathbf{X}_a^{i-1}\mathbf{X}_a^i\mathbf{X}_0^i$ shaded in red. A second imaginary four bar (seen in green) is assumed such that $\angle\mathbf{X}_a^i\mathbf{X}_0^i\bar{\mathbf{X}}_b^i = \pi/2$ and $\bar{\mathbf{X}}_b^{i-1}$ is directly below $\bar{\mathbf{X}}_b^i$. In the above mentioned four bars, the fixed linkages are $\mathbf{X}_0^{i-1}\mathbf{X}_a^{i-1}$ and $\mathbf{X}_0^{i-1}\bar{\mathbf{X}}_b^{i-1}$, and the couplers are $\mathbf{X}_0^i\mathbf{X}_a^i$ and $\mathbf{X}_0^i\bar{\mathbf{X}}_b^i$ with $\mathbf{X}_0^{i-1}\mathbf{X}_0^i$ being the first crank for both.

After actuation of the cable, the backbone deforms and the position vectors $\mathbf{X}^i_{(.)}$ changes to $\mathbf{x}^i_{(.)}$ (see Figure 2b). The position after actuation can be found out by simultaneously minimizing both the coupler angles which can be mathematically stated as the following minimization problem:

$$\underset{\mathbf{x}^i_0, \mathbf{x}^i_a}{\arg\min} \left(\left[\arccos\left(\frac{\mathbf{A}}{\|\mathbf{A}\|} \cdot \frac{\mathbf{B}}{\|\mathbf{B}\|} \right) \right]^2 + \left[\arccos\left(\frac{\mathbf{C}}{\|\mathbf{C}\|} \cdot \frac{\mathbf{D}}{\|\mathbf{D}\|} \right) \right]^2 \right) \tag{1}$$

where, $\mathbf{A} = \mathbf{X}^{i-1}_0 - \mathbf{X}^{i-1}_a$, $\mathbf{B} = \mathbf{x}^i_0 - \mathbf{x}^i_a$, $\mathbf{C} = \mathbf{X}^{i-1}_0 - \bar{\mathbf{X}}^{i-1}_b$, $\mathbf{D} = \mathbf{x}^i_0 - \bar{\mathbf{x}}^i_b$

Subject to:

$$\begin{gathered} \|\mathbf{x}^i_0 - \mathbf{X}^{i-1}_0\| = l_0, \quad \|\mathbf{x}^i_a - \mathbf{X}^{i-1}_a\| = l^i_a, \quad \|\mathbf{x}^i_0 - \mathbf{x}^i_a\| = a, \\ \bar{\mathbf{X}}^i_b = a \frac{\left(\mathbf{X}^i_a - \mathbf{X}^i_0\right) \times \left(\mathbf{X}^i_0 - \mathbf{X}^{i-1}_0\right)}{\| \left(\mathbf{X}^i_a - \mathbf{X}^i_0\right) \times \left(\mathbf{X}^i_0 - \mathbf{X}^{i-1}_0\right) \|} \end{gathered} \tag{2}$$

Given data: $\mathbf{X}^i_0, \mathbf{X}^{i-1}_0, \mathbf{X}^i_a, \mathbf{X}^{i-1}_a, l_0, l^i_a, a$

Equation 1, along with the constraints, need to be solved starting from the base till the tip sequentially such that output of each step (the position of the coupler) becomes the base of the four bar for the next segment.

Cosserat rod model: In the Cosserat rod model [9], the backbone is assumed to be a parametric space curve with a parameter $s \in [0, L]$, where L is the total length of the CCR. The position of any point on the backbone can be represented as a vector $\boldsymbol{p}(s)$ and the local coordinate system, similar to a Frenet–Serret frame, is represented as $\boldsymbol{R}(s)$ (see Fig. 2c). The location of the cable in the local coordinate system is denoted by $\boldsymbol{r}_i(s)$. It is assumed that $\boldsymbol{r}_i(s)$ does not change with actuation and the internal force is always tangent to the cable position, $\boldsymbol{p}_i(s)$. With $\boldsymbol{p}(s)$, $\boldsymbol{R}(s)$ and their respective rate of change with respect to s, $\boldsymbol{v}(s)$ and $\boldsymbol{u}(s)$, one can solve for a set of first order differential equations (ODEs) obtained from the constitutive relations to get the pose of the CCR after actuation. The first-order ODEs are given by

$$\begin{gathered} \dot{\boldsymbol{p}} = \boldsymbol{R}\boldsymbol{v}, \quad \begin{bmatrix} \dot{\boldsymbol{v}} \\ \dot{\boldsymbol{u}} \end{bmatrix} = \begin{bmatrix} \boldsymbol{K}_{se} + \boldsymbol{A} & \boldsymbol{G} \\ \boldsymbol{G}^T & \boldsymbol{K}_{bt} + \boldsymbol{H} \end{bmatrix}^{-1} \begin{bmatrix} \boldsymbol{d} \\ \boldsymbol{c} \end{bmatrix} \\ \dot{\boldsymbol{R}} = \boldsymbol{R}\widehat{\boldsymbol{u}}, \end{gathered} \tag{3}$$

where,

$$\boldsymbol{c} = -\widehat{\boldsymbol{u}}\boldsymbol{K}_{bt}\boldsymbol{u} - \widehat{\boldsymbol{v}}\boldsymbol{K}_{se}\left(\boldsymbol{v} - [0,0,1]^T\right) - \boldsymbol{b},\ \boldsymbol{b} = \sum_{i=1}^{n} \widehat{\boldsymbol{r}}_i A_i \left(\widehat{\boldsymbol{u}}\dot{\boldsymbol{p}}^b_i + \widehat{\boldsymbol{u}}\dot{r}_i + \ddot{\boldsymbol{r}}_i\right)$$

$$\boldsymbol{d} = -\widehat{\boldsymbol{u}}\boldsymbol{K}_{se}\left(\boldsymbol{v} - [0,0,1]^T\right) - \boldsymbol{a},\ \boldsymbol{a} = \sum_{i=1}^{n} A_i \left(\widehat{\boldsymbol{u}}\dot{\boldsymbol{p}}^b_i + \widehat{\boldsymbol{u}}\dot{r}_i + \ddot{\boldsymbol{r}}_i\right)$$

$$A_i = -\tau_i \left(\widehat{\dot{\boldsymbol{p}}}^b_i\right)^2 / \left\|\dot{\boldsymbol{p}}^b_i\right\|^3,\ \boldsymbol{A} = \sum_{i=1}^{n} A_i,\ \boldsymbol{G} = -\sum_{i=1}^{n} A_i \widehat{\boldsymbol{r}}_i,\ \boldsymbol{H} = -\sum_{i=1}^{n} \widehat{\boldsymbol{r}}_i A_i \widehat{\boldsymbol{r}}_i$$

and $\widehat{(\cdot)}$ represents the skew-symmetric matrix made by the elements of $(\cdot)$, $\boldsymbol{K}_{se}$ and $\boldsymbol{K}_{bt}$ are the stiffness matrix for extension/shear and bending, respectively. τ_i is the load. Superscript 'b' denotes the vector in the local coordinate system.

The boundary conditions for $\boldsymbol{p}(s)$ and $R(s)$ are known at the base. At the tip, the cable termination applies a force and moment on the backbone which produces the boundary conditions for $\boldsymbol{v}(s)$ and $\boldsymbol{u}(s)$. The ordinary differential equations and the boundary conditions form a boundary value problem.

3 Comparison between optimization and Cosserat rod models

We compare the optimization and the Cosserat rod model for a CCR of length, $L = 180$ mm with 9 equal segments (10 disks). Each disk has 12 holes, equally spaced along a circle of radius, $a = 8$ mm. Out of the several numerical simulations, the results for four of them are presented in Table 1. 'Cable positions' denote the location of the cable in a particular disk according to the nomenclature in the inset of Fig 1, starting from the bottom to the tip of the CCR. For each case, the load applied was 400 grams and the corresponding change in length of the cable inside the CCR (found out experimentally) denoted as '% Cable actuation' is presented in Table 1. All the simulations were performed using MATLAB in a PC with an Intel processor (3.1 GHz) and 16 GB RAM.

Table 1 Cable routings used for comparison

Case	Type	Cable position	% Cable actuation	RMS Error (mm)	
				Optimization	Cosserat
I	Straight	4-4-4-4-4-4-4-4-4-4	5.5	1.79	2.08
II	Helical	1-2-3-4-5-6-7-8-9-10	7.0	1.85	1.87
III	General	1-2-3-4-4-4-4-3-2-1	5.7	1.44	1.80
IV	General	10-10-10-10-10-10-11-12-1-2	5.3	1.37	1.90

Numerical simulation details: For the optimization-based method, equation 1 is solved using `fmincon` (available in MATLAB) with the in-built *interior-point* algorithm. For each section a total of 6 variables are solved. The boundary value problem for Cosserat rod model is solved using *shooting method* [15] for a total of 18 state variables. The cable positions, $\boldsymbol{r}_i(s)$ are provided as an 8^{th} order Fourier approximations so that it is $\mathcal{C}^2$ continuous. For both cases, the initial guesses provided for the simulations are the values of the particular variables when the CCR was unactuated.

A sample simulation result for Case III is shown in Fig 3a. For this simulation, the optimization based method took 2.20 seconds, where as it took 10.07 seconds for the Cosserat rod model.

Experimental setup and error comparison: To compare both the models experimentally, a CCR prototype was 3D printed in ABS material ($E = 1.1$ GPa, $\nu = 0.3$) with the dimensions as specified in the beginning of section 3.

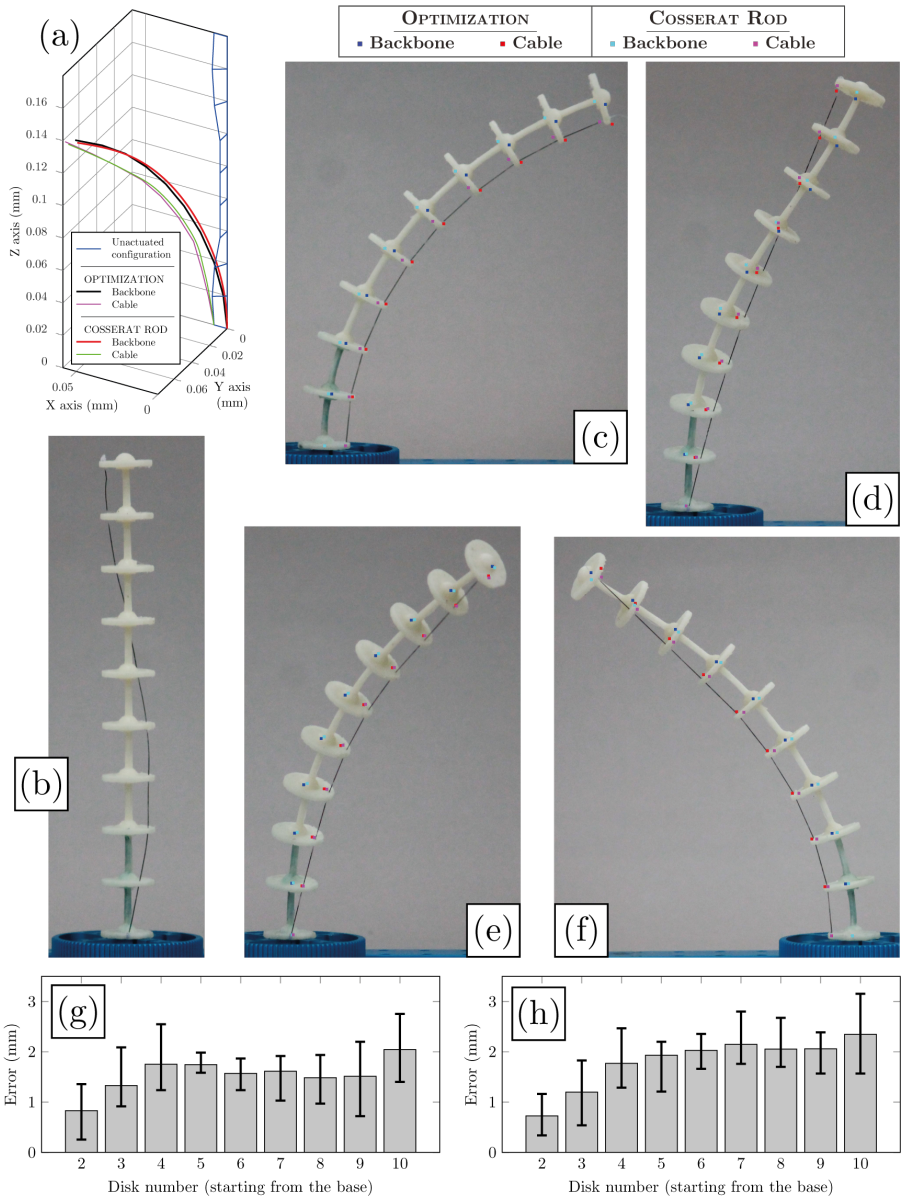

Fig. 3 (a) Simulation result for Case III. (b) Experimental setup. Comparison of experimental results for (c) Case I (d) Case II (e) Case III and (f) Case IV. Error at each disk as compared with the experiments for (g) Optimization-based and, (h) Cosserat rod model.

Thin nylon wires are used as cables for the CCR and 400 gram weight is used to actuate these cables. The experimental setup for Case II before actuation is shown in Fig. 3b. The corresponding change in cable length inside the CCR is measured externally and is presented as '% Cable actuation' in Table 1.

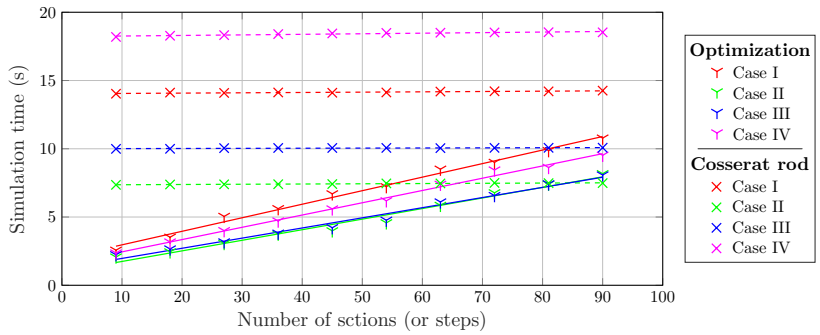

Fig. 4 Variation of simulation time vs number of sections (or step size)

An image of the CCR is captured before and after actuation and then the simulation results are superimposed on the captured image which are shown as blue, cyan, magenta and red dots in the Fig. 3(c)-(f).

The error in each case is found out by image processing. The mean error at each disk is shown in Fig. 3(g)-(h). The RMS error for each case is presented in Table 1. From both the error comparison, it can be seen that both the models can predict the shape of the robot accurately with maximum RMS error of 1.85 mm and 2.08 mm for optimization and Cosserat rod models, respectively. It was observed that in most cases the optimization-based method is more accurate in predicting the shape than the Cosserat rod model.

Comparison of computation time against number of sections: A comparison of computation time for simulation based on the number of sections (or number of steps for Cosserat rod model), for a fixed length of CCR, was performed for the routings presented in Table 1. Each model is simulated six times and gradually increasing the number of sections, keeping the length constant. The mean value of the results are presented in Fig. 4 as scatter plot and then a linear fit is applied to the data points. It can be seen that computation time increases linearly for the optimization-based model, but does not vary significantly for the Cosserat rod model. Hence, it is advantageous to use the Cosserat rod model when there is need for large number of sections. However, typically the number of sections is within 20, and the optimization-based method is faster is most of these cases. The simulation times for the optimization-based method can be further reduced if one provides the gradients as an input to `fmincon`.

4 Conclusion

In this paper we have presented a comparison of two modelling approaches for the shape-prediction of a cable-driven continuum robot (CCR). The optimization-based method is based on geometry, so it does not require the material properties as in the Cosserat rod model and it is significantly faster in most simula-

tions. Even though Cosserat rod model requires elastic properties for kinematic analysis, the accuracy of the results are comparable with the optimization-based method. Based on this work, we can conclude that one should opt for the optimization-based method when the material properties are not known or hard to determine and when one needs faster simulation as in a possible model-based control scheme. However, for CCRs with large number of segments (more than 50), one may choose Cosserat rod model for calculations. Both the models predict the shape of the CCR reasonably accurately for the experiments performed in this work (with RMS error less than 2.1 mm). The optimization-based method is currently being extended to include other configurations of the CCR and to further reduce the simulation time for a model-based controller.

Conflict of interest

The authors declare that they have no conflict of interest.

Acknowledgement

The 3D printing of the CCR was done at the Design Innovation Center (DIC), UTSAAH Laboratory both at the Centre for Product Design and Manufacturing, Indian Institute of Science, Bangalore. The authors thank the help provided at these labs.

References

1. Kolachalama, S., Lakshmanan, S.: Continuum robots for manipulation applications: A survey. Journal of Robotics **2020**, 1–19 (2020)
2. Robert J. Webster, I., Jones, B.A.: Design and kinematic modeling of constant curvature continuum robots: A review. The International Journal of Robotics Research **29**(13), 1661–1683 (2010)
3. Rao, P., Peyron, Q., Lilge, S., Burgner-Kahrs, J.: How to model tendon-driven continuum robots and benchmark modelling performance. Frontiers in Robotics and AI **7** (2021)
4. Gravagne, I., Walker, I.: On the kinematics of remotely-actuated continuum robots. In: Proceedings 2000 ICRA. Millennium Conference. IEEE International Conference on Robotics and Automation. Symposia Proceedings, vol. 3, pp. 2544–2550 (2000)
5. Bieze, T.M., Kruszewski, A., Carrez, B., Duriez, C.: Design, implementation, and control of a deformable manipulator robot based on a compliant spine. The International Journal of Robotics Research **39**(14), 1604–1619 (2020)
6. Grazioso, S., Gironimo, G.D., Siciliano, B.: A geometrically exact model for soft continuum robots: The finite element deformation space formulation. Soft Robotics **6**(6), 790–811 (2019)
7. Yuan, H., Zhou, L., Xu, W.: A comprehensive static model of cable-driven multi-section continuum robots considering friction effect. Mechanism and Machine Theory **135**, 130–149 (2019)
8. Oliver-Butler, K., Till, J., Rucker, C.: Continuum robot stiffness under external loads and prescribed tendon displacements. IEEE Transactions on Robotics **35**(2), 403–419 (2019)

9. Rucker, D.C., Webster III, R.J.: Statics and dynamics of continuum robots with general tendon routing and external loading. IEEE Transactions on Robotics **27**(6), 1033–1044 (2011)
10. Dehghani, M., Moosavian, S.A.A.: Modeling of continuum robots with twisted tendon actuation systems. In: 2013 First RSI/ISM International Conference on Robotics and Mechatronics (ICRoM), pp. 14–19 (2013)
11. Mishra, A.K., Mondini, A., Del Dottore, E., Sadeghi, A., Tramacere, F., Mazzolai, B.: Modular continuum manipulator: analysis and characterization of its basic module. Biomimetics **3**(1), 3 (2018)
12. Dalvand, M.M., Nahavandi, S., Howe, R.D.: An analytical loading model for n -tendon continuum robots. IEEE Transactions on Robotics **34**(5), 1215–1225 (2018)
13. Liu, Z., Zhang, X., Cai, Z., Peng, H., Wu, Z.: Real-time dynamics of cable-driven continuum robots considering the cable constraint and friction effect. IEEE Robotics and Automation Letters **6**(4), 6235–6242 (2021)
14. Ashwin, K.P., Ghosal, A.: Profile estimation of a cable-driven continuum robot with general cable routing. In: Advances in Mechanism and Machine Science, pp. 1879–1888. Springer International Publishing (2019)
15. Till, J., Aloi, V., Rucker, C.: Real-time dynamics of soft and continuum robots based on cosserat rod models. The International Journal of Robotics Research **38**(6), 723–746 (2019)